BEILSTEIN JOURNAL OF NANOTECHNOLOGY

Temperature-dependent Raman spectroscopy and sensor applications of $PtSe_2$ nanosheets synthesized by wet chemistry

Mahendra S. Pawar[1,2] and Dattatray J. Late[*1,2]

Full Research Paper

Open Access

Address:
[1]Physical and Materials Chemistry Division, CSIR-National Chemical Laboratory, Dr. Homi Bhabha Road, Pune 411008, India and
[2]Academy of Scientific and Innovative Research (AcSIR), Ghaziabad 201002, India

Email:
Dattatray J. Late[*] - dj.late@ncl.res.in

* Corresponding author

Keywords:
nanosheets; $PtSe_2$; Raman spectroscopy; sensor; thermal effect

Beilstein J. Nanotechnol. **2019,** *10,* 467–474.
doi:10.3762/bjnano.10.46

Received: 01 November 2018
Accepted: 16 January 2019
Published: 13 February 2019

This article is part of the thematic issue "Low-dimensional materials and systems".

Guest Editor: S. Walia

Abstract

We report on a wet chemistry method used to grow $PtSe_2$ nanosheets followed by thermal annealing. The SEM and TEM analysis confirms the formation of $PtSe_2$ nanosheets. Furthermore, XRD, Raman, XPS and SAED patterns were used to analyze the crystal structure and to confirm the formation of the $PtSe_2$ phase. The temperature-dependent Raman spectroscopy investigations were carried out on $PtSe_2$ nanosheets deposited on Si substrates in the temperature range 100–506 K. The shifts in Raman active E_g and A_{1g} modes as a function of temperature were monitored. The temperature coefficient for both modes was calculated and was found to match well with the reported 2D transition metal dichalcogenides. A $PtSe_2$ nanosheet-based sensor device was tested for its applicability as a humidity sensor and photodetector. The humidity sensor based on $PtSe_2$ nanosheets showed an excellent recovery time of ≈5 s, indicating the great potential of $PtSe_2$ for future sensor devices.

Introduction

Graphene, the most well-studied example of the two-dimensional (2D) aromatic compounds, is the building block of all forms of carbon allotropes [1]. In recent years, it has been widely studied due to its extraordinary optical, electrical, mechanical, magnetic and chemical properties [2-5]. Like graphene and its organic analogues [6], inorganic 2D metal dichalcogenides also exhibit outstanding performance in many applications including transistors, sensors, photodetectors, solar cells, field emitters, battery materials, light harvesting and energy storage devices, catalyst for H_2 generation, and drug delivery applications [7-12]. Most of the transition metal dichalcogenides (TMDCs) are semiconducting in nature with MX_2 type – where M is a metal, M = W, Mo, Sn, Nb, V, etc. from group IV–V and X represents the chalcogenides family, X = S, Se, Te, etc. The metal atom M is sandwiched between layers of chalcogenide (X) atoms in the structure X–M–X. The

TMDCs show diverse functional properties at the monolayer level in contrast to bulk due to the quantum confinement effect. Apart from this, these TMDCs, for example MoS_2 and $MoSe_2$, show an indirect to direct band gap transition [13-17].

A 2D platinum diselenide ($PtSe_2$) material has recently joined the growing class of stable TMDCs due its promising applications. The 2D $PtSe_2$ has not been explored much to date due to difficulties in synthesis. It is well known that bulk $PtSe_2$ is a semimetal in nature with a nearly zero band gap [18,19]. With the help of theoretical calculations such as density functional theory (DFT) and local-density approximations (LDAs), it has been observed that bulk $PtSe_2$ shows a semimetallic nature and single-layer $PtSe_2$ has a semiconducting nature with a bandgap of 1.2 eV. Bilayer $PtSe_2$ is also a semiconducting material but with a slightly smaller band gap than the monolayer material [19]. This layer-dependent conversion of semimetal-to-semiconductor transition has potential for electronic device applications [20-22]. Bulk $PtSe_2$ was first prepared in 1909 by Minozzi from elements [23]. $PtSe_2$ nanosheets have been recently prepared by heating thin foils of platinum in selenium vapors at 400 °C [19,24]. In this paper we have synthesized few-layer-thick $PtSe_2$ nanosheets by a wet chemical method [25] at 90 °C using chloroplatinic acid (H_2PtCl_6) and Se powder as precursors followed by thermal annealing at 500 °C. Temperature-dependent Raman spectroscopic characterization was carried out on the materials.

Materials and Methods

All the chemicals such as chloroplatinic acid, Se powder, hexamethylenetetramine, and $NaBH_4$ were purchased from Sigma-Aldrich for the synthesis of $PtSe_2$ nanosheets.

Synthesis method

The $PtSe_2$ nanosheets were synthesized using a solvothermal method followed by annealing at 500 °C using a previously described method for $PtSe_2$ synthesis [25]. The $PtSe_2$ material was prepared in two steps. The first step is the formation of the PtSe complex on the wall of a container by a wet chemical method; the second step is the phase transformation of $PtSe_2$ by thermal annealing. 0.5 mL of a 0.015 M solution of H_2PtCl_6 was mixed with 0.5 mL of 0.5 M hexamethylenetetramine. In order to get a homogeneous solution, the mixture was carefully stirred for 15–20 s until the colour of the solution became slightly yellow; this is referred to as the Pt precursor. In another beaker 0.8 mg of Se powder was added into a 10 mL ice-cold solution of 0.1 M $NaBH_4$ which acts as a strong reducing agent for the reduction of Se powder. The solution of Se was then heated in an oil bath at 90 °C for ≈20 min in order to completely reduce the Se. After complete reduction, the colour of the solution became dark brown and is referred to as the Se precursor. The Pt precursor was then slowly added into the Se precursor. The colour of the solution was found to suddenly change to greenish brown. The mixture was then kept undisturbed for ≈20 min. After 20 min the complex of Pt and Se was formed on the wall of the beaker. The complex was then washed several times using deionized water. First complex was transferred onto a Si substrate and heated at 100 °C on a hot plate. After complete evaporation, the substrate was annealed in a chemical vapour deposition system at 500 °C in argon gas atmosphere for 5 h. Supporting Information File 1, Figure S1 shows the schematic of the $PtSe_2$ nanosheet synthesis steps.

Sensor device fabrication and testing

Sensor devices were fabricated on a tin-doped indium oxide (ITO) substrate with a channel length of ≈300 μm and width ≈5 mm. The $PtSe_2$ nanosheet powder was dispersed in *N*-methyl-2-pyrrolidone (NMP) solvent and then drop casted between the channels. The devices were further annealed in a vacuum furnace at 170 °C to improve the contact resistance and adhesion of the nanosheets with the substrate. The humidity sensing performance was investigated by exposing the sensor device to various relative humidity (RH) levels ranging from 11.3–97.3% as described in detail previously [26]. All of the electrical tests such as current–voltage (*I*–*V*) and current–time (*I*–*t*) measurements were carried out using a Keithley 2612A system source meter which was attached to a computer through a GPIB 488A interface. For the photodetection study, a green LED was used. All sensor experiments were carried out at ambient pressure and room temperature.

Results and Discussion

Structural characterization

The structural characterization was carried out using X-ray diffraction (XRD) and Raman spectroscopy. Figure 1a shows the typical XRD pattern of the as-prepared sample deposited on a Si substrate. XRD was performed on a PANalytical X'pert pro dual goniometer diffractometer using Cu Kα radiation. The samples were mounted flat and scanned between 10 to 60°. The XRD pattern of the as-prepared sample shows the strong characteristic peaks around $2\theta = 17.41°$ and 33.17° belonging to the (001) and (011) planes of $PtSe_2$. These values match well with the JCPDS data card number (88-2281) and as observed in a previous report [27]. Figure 1b shows the Raman spectra of the as-prepared few-layer $PtSe_2$ nanosheets. The Raman spectra were recorded using a Renishaw microscope at a wavelength of 532 nm with laser power ≈25 mW and laser spot diameter ≈1 μm. The typical Raman spectra recorded at room temperature consist of two distinct peaks, one at ≈176 cm^{-1} corresponding to the E_g mode and another slightly less intense peak at ≈205 cm^{-1} corresponding to the A_{1g} mode. The E_g mode in the Raman spectra corresponds to in-plane vibration due to the

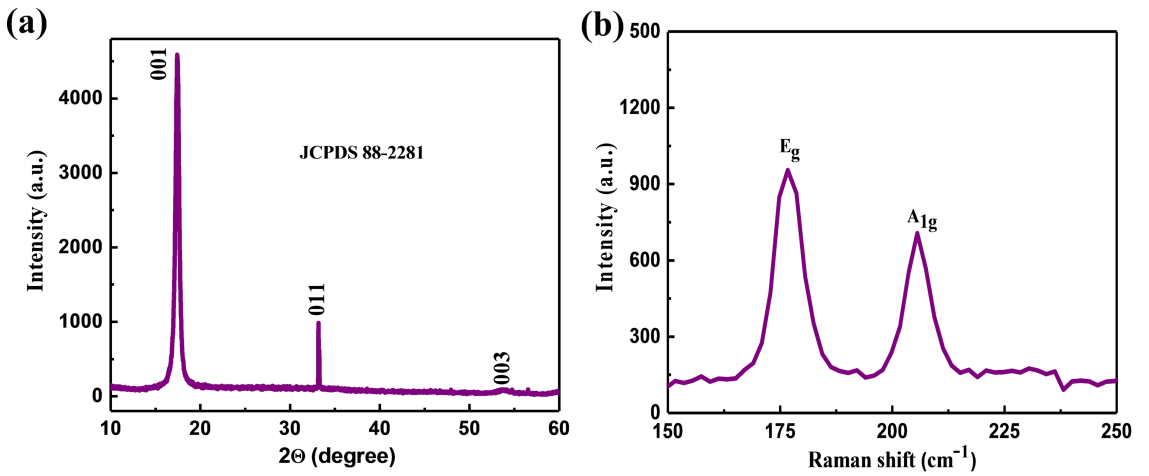

Figure 1: $PtSe_2$ nanosheets. (a) Typical XRD pattern and (b) Raman spectra recorded at room temperature.

opposite motion of the upper and lower Se atoms. The A_{1g} mode in the Raman spectra corresponds to the out-of-plane vibration of Se atoms [22,28].

Morphological investigations were carried out using scanning electron microscopy (SEM). Figure 2a–c shows SEM images of few-layer $PtSe_2$ with typical overlapping of multiple sheets on

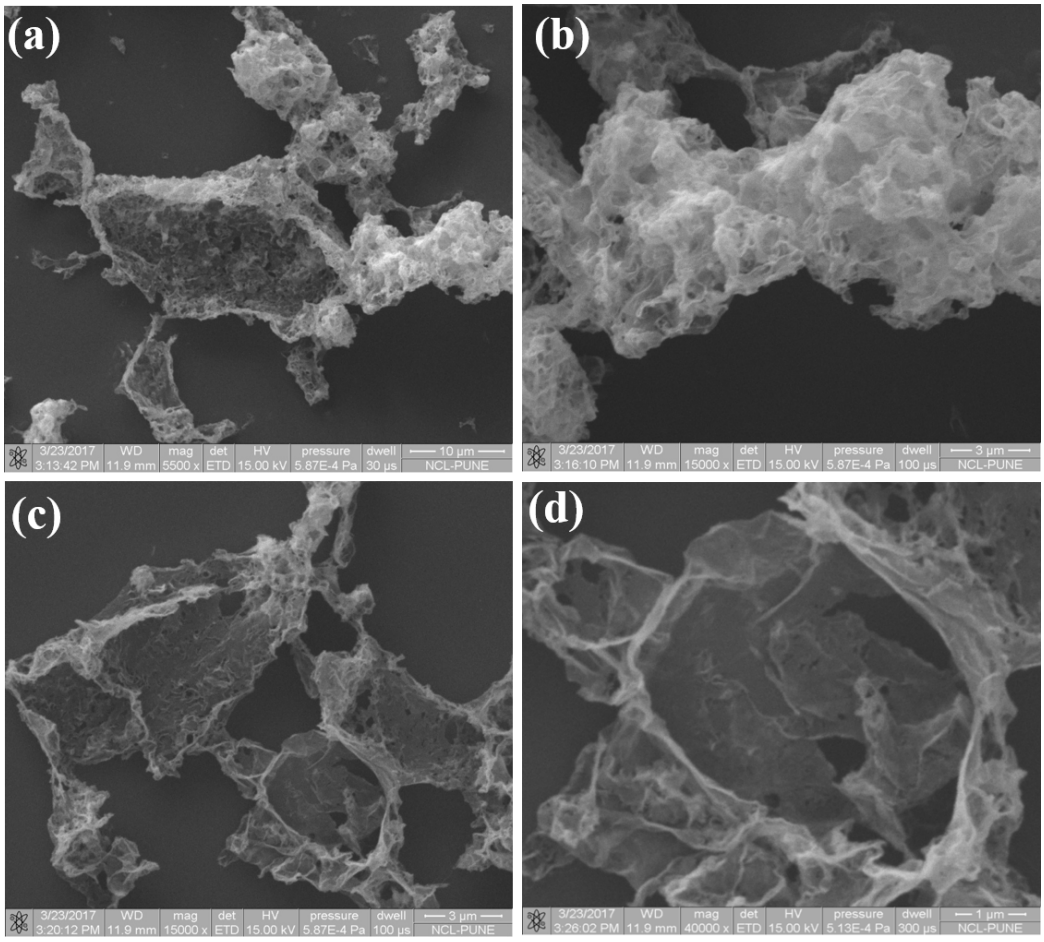

Figure 2: (a–d) Typical SEM images for $PtSe_2$ nanosheets synthesized using the wet chemistry method.

each other. Figure 2d shows an SEM image indicating a more transparent thin layer of $PtSe_2$ stacked on each other, exhibiting the few-layer nature of the as-synthesized $PtSe_2$ sample. Figure 3a–c shows the low-resolution TEM images of the as-synthesized $PtSe_2$ sample clearly showing the sheet-like morphology with lateral dimension of ≈700 nm. Figure 3d shows a high-resolution TEM image of the $PtSe_2$ nanosheets. The inset of Figure 3d shows the selected area electron diffraction pattern (SAED) which depicts the crystalline nature of the as-synthesized $PtSe_2$ sample. The X-ray photoelectron spectroscopy (XPS) spectra of the Pt 4f and Se 3d regions acquired on a $PtSe_2$ nanosheet sample were carried out on a film deposited on the Si substrate. The Figure 4a represents the fitted spectrum for Pt $4f_{7/2}$ and Pt $4f_{5/2}$ with binding energy 72.55 eV and 75.83 eV, respectively. Similarly, for Se, the binding energy spectrum can be fitted by Gaussian–Lorentzian curves shown in Figure 4b. The two peaks with binding energy 54.8 eV and 55.6 eV are observed for the $3d_{5/2}$ and $3d_{3/2}$ states, respectively. There is one more peak observed in the Se region with low intensity at 52.9 eV which corresponds to Pt $5d_{3/2}$ [24]. The thickness of the as-prepared $PtSe_2$ nanosheets was calculated using atomic force microscopy (AFM). Figure 5a shows the AFM image which clearly shows that the lateral dimensions of the nanosheets are ≈700 nm. Figure 5b represents the corresponding height profile plot for the $PtSe_2$ nanosheet with thickness found to be ≈47 nm.

Temperature-dependent Raman spectroscopy of few-layer $PtSe_2$ nanosheets

The temperature-dependent Raman spectroscopy investigations of few-layer $PtSe_2$ nanosheets were carried out between 100–506 K. The Raman spectra of the $PtSe_2$ nanosheets at different temperatures are provided in Supporting Information File 1, Figures S2 and S3. The Raman mode E_g and A_{1g} as a function of temperature is shown in Figure 6a,b. It can be clearly seen that the position of the A_{1g} and E_g modes shifts to

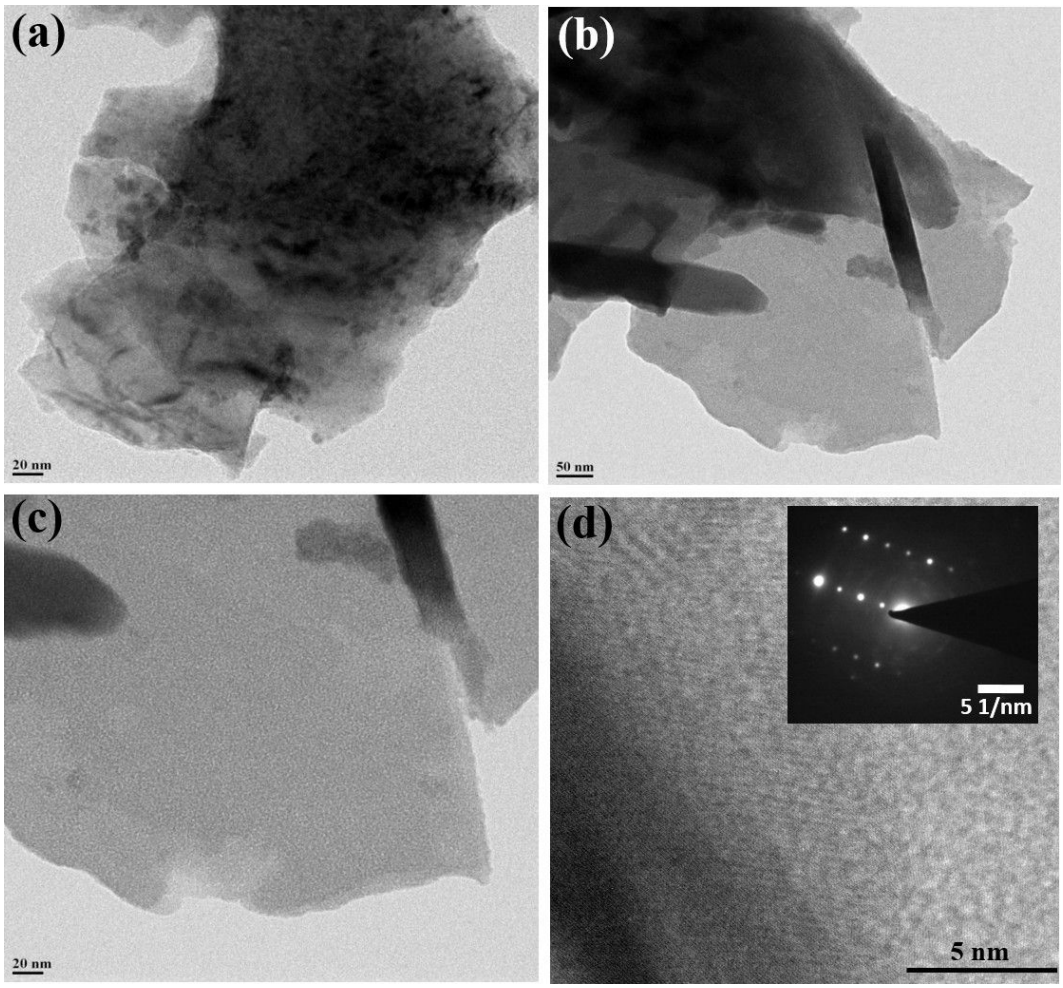

Figure 3: (a–c) Low-magnification TEM images and (d) a high-magnification TEM image, where the inset shows the selected area electron diffraction (SAED) pattern for the as-synthesized $PtSe_2$ nanosheets.

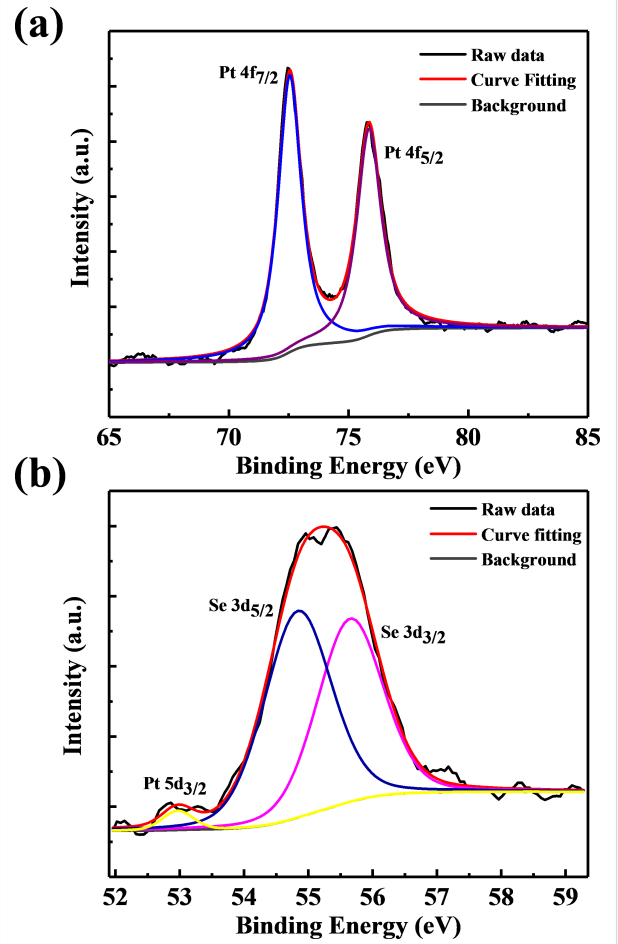

Figure 4: (a) Deconvoluted XPS spectra for Pt and (b) Se elements.

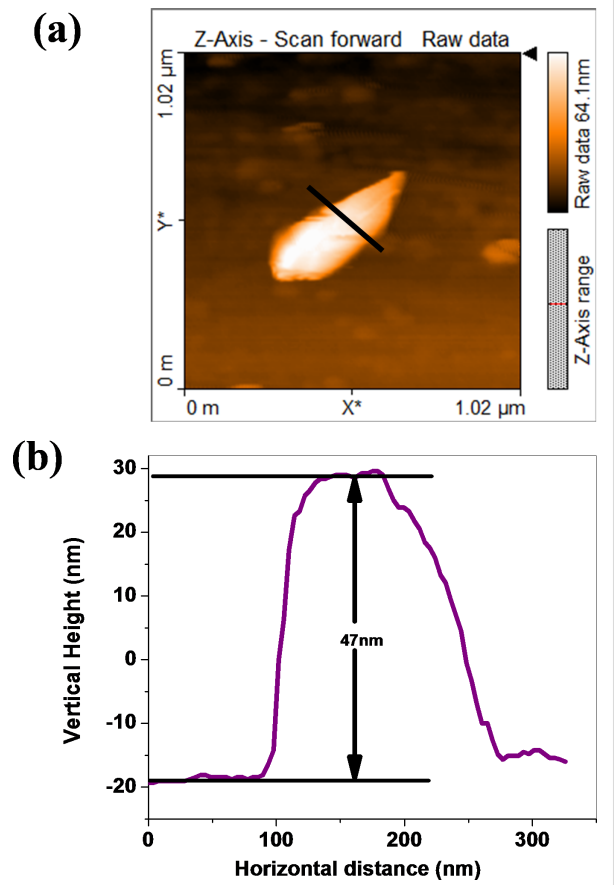

Figure 5: (a) AFM image and (b) AFM height profile plot for a $PtSe_2$ nanosheet.

lower wavenumbers as the temperature increases from 100 K to 506 K. The Raman modes E_g and A_{1g} for $PtSe_2$ behave linearly within the temperature range 100–506 K. Furthermore, it was observed that the full width half maximum (FWHM) increases with an increase in temperature. The peak positions in the Raman spectra were calculated by fitting the Lorentzian function to the A_{1g} and E_g modes. The temperature coefficient can be calculated by Equation 1 [29]:

$$\omega(T) = \omega_0 + \chi T\,, \tag{1}$$

where ω_0 is the peak position of the A_{1g} and E_g mode at zero Kelvin, χ is the temperature coefficient of the A_{1g} and E_g modes, and ω is a Raman phonon frequency. The slope of the Raman modes vs temperature plot directly gives the value of the temperature coefficient and is given in Table 1. Further, it was clearly seen that the Raman peak position and peak broadening was affected by temperature. This change in Raman modes is mainly due to the contribution from the thermal anharmonicity.

The Raman phonon frequency as a function of volume and temperature is given by Equation 2 [30]:

$$\left(\frac{\partial \ln\omega}{\partial T}\right)_P = \left(\frac{\partial \ln V}{\partial T}\right)_P \left(\frac{\partial \ln\omega}{\partial \ln V}\right)_T + \left(\frac{\partial \ln\omega}{\partial T}\right)_V$$
$$\left(\frac{\partial \ln\omega}{\partial T}\right)_P = -\frac{\gamma}{K}\left(\frac{\partial \ln\omega}{\partial P}\right)_T + \left(\frac{\partial \ln\omega}{\partial T}\right)_V \tag{2}$$

where γ is the volume thermal coefficient and K represents the isothermal volume compressibility. The first term on the right hand side, $-\gamma/K\,(\partial \ln\omega/\partial P)_T$, represents the volume contribution at a constant temperature. The second term, $(\partial \ln\omega/\partial T)_V$, represents the temperature contribution at constant volume. In single-layer TMDCs due to the direct band gap, the double resonance phenomenon is useful to explain the change in FWHM, intensity and the peak shift as a function of temperature. The double resonance phenomenon can be attributed to several process including absorption of an incident photon, creation of a hole pair,

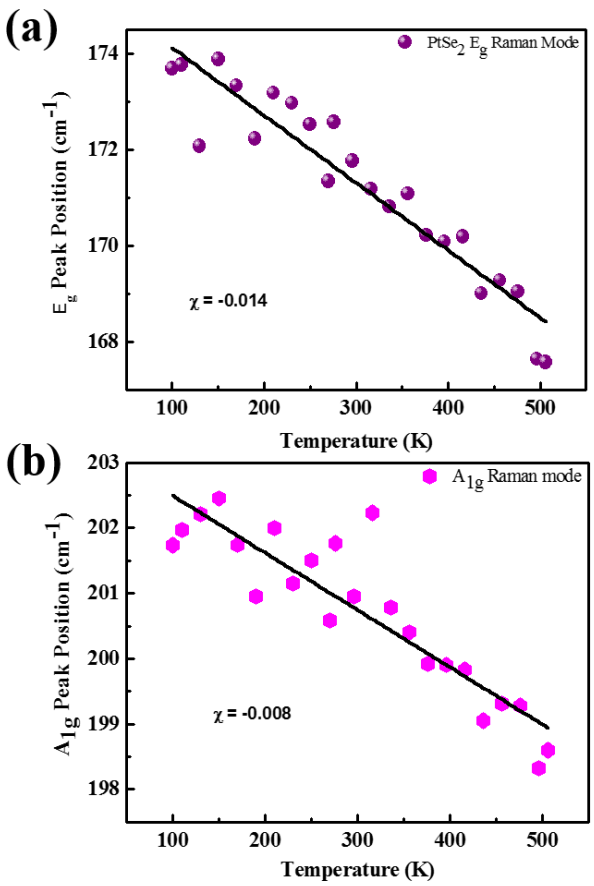

Figure 6: Temperature-dependent Raman spectra analysis for $PtSe_2$ nanosheets for the (a) E_g mode and the (b) A_{1g} mode as a function of temperature.

Table 1: Temperature coefficient values for the A_{1g} and E_g modes in a $PtSe_2$ nanosheet sample.

Material	Raman modes	Temperature coefficient (χ)	Δω (cm^{-1})
$PtSe_2$ nanosheet	E_g	−0.014	6.11
	A_{1g}	−0.008	3.14

double scattering of a created hole pair by phonon, and recombination of an electron–hole pair with emission of phonon. The temperature coefficient for the E_g and A_{1g} modes was found to be −0.014 and −0.008, respectively. The nature of the temperature dependence of the Raman spectra of $PtSe_2$ nanosheets is found to be similar in nature to that of graphene and other 2D materials such as MoS_2, WS_2, $MoSe_2$, WSe_2, BP, TiS_3, multilayer graphene, and $MoTe_2$ [29,31-34]. A comparison of the temperature coefficient values corresponding to various 2D materials are shown in Table 2. The value of Δω for both E_g and A_{1g} modes was found to be 6.11 cm^{-1} and 3.14 cm^{-1}, respectively.

Table 2: Temperature coefficient values for various 2D materials.

TMDCs	Raman modes	Temperature coefficient (χ)	Δω (cm^{-1})	Ref.
$MoSe_2$	A_{1g}	−0.0096	4.75	[29]
WSe_2	A_{1g}	−0.0071	3.81	[29]
MoS_2	E_g	−0.0136	8	[29]
	A_{1g}	−0.0113	6.11	
WS_2	E_g	−0.0098	4.51	[29]
	A_{1g}	−0.014	6.43	
black phosphorous	A_{1g}	−0.008	4.39	[31]
	B_{2g}	−0.013	8.14	
	A_{2g}	−0.014	8.63	
TiS_3	A_{1g}	−0.022, −0.025, −0.024, −0.017	–	[32]
single-layer graphene	G	−0.0162	–	[33]
bilayer graphene	G	−0.0154	–	
$MoTe_2$ (bilayer)	E'_{2g}	−0.0116	–	[34]
	B'_{2g}	−0.0181	–	
$PtSe_2$	E_g	−0.014	6.11	this work
	A_{1g}	−0.008	3.14	

Humidity sensor and photodetector based on few-layer $PtSe_2$ nanosheets

Figure 7a shows the typical resistance of the sensor device vs relative humidity plot. The resistance is significantly decreased from 3.75 GΩ to 0.83 MΩ. The humidity sensing mechanism for the $PtSe_2$ sensor can be explained as follows. When the $PtSe_2$ nanosheet sensor device was exposed to water molecules/vapors, a charge transfer between the water molecules and the $PtSe_2$ nanosheets occurs. This results in the decrease in resistance of the $PtSe_2$ nanosheet sensor device with an increase in the relative humidity. The interactions among the water molecules (electron donor) and the $PtSe_2$ nanosheets results in an enhancement in the conductivity of the sensor device, similar to that observed for other 2D materials such as $SnSe_2$ [35], MoS_2 [36], BP [26], and $MoSe_2$ [37]. Figure 7b shows a typical current–time (*I*–*t*) plot where cycles of 11.3% and 97.3% RH levels were used to calculate the response and recovery time. The response and recovery time for the $PtSe_2$-based humidity sensor device was found to be 118 s and 5 s, respectively. The advantage of the $PtSe_2$-based humidity sensor device is its rapid recovery and its functionality at room temperature. Figure 7c shows a typical *I*–*V* plot in dark conditions and under green light illumination. Figure 7d shows the *I*–*t* plot for the photodetector based on $PtSe_2$ nanosheets with a response time of ≈110 s and a recovery time of ≈129 s.

Conclusion

In conclusion, we report on a wet chemistry method to grow $PtSe_2$ nanosheets. The SEM and TEM analysis confirm the for-

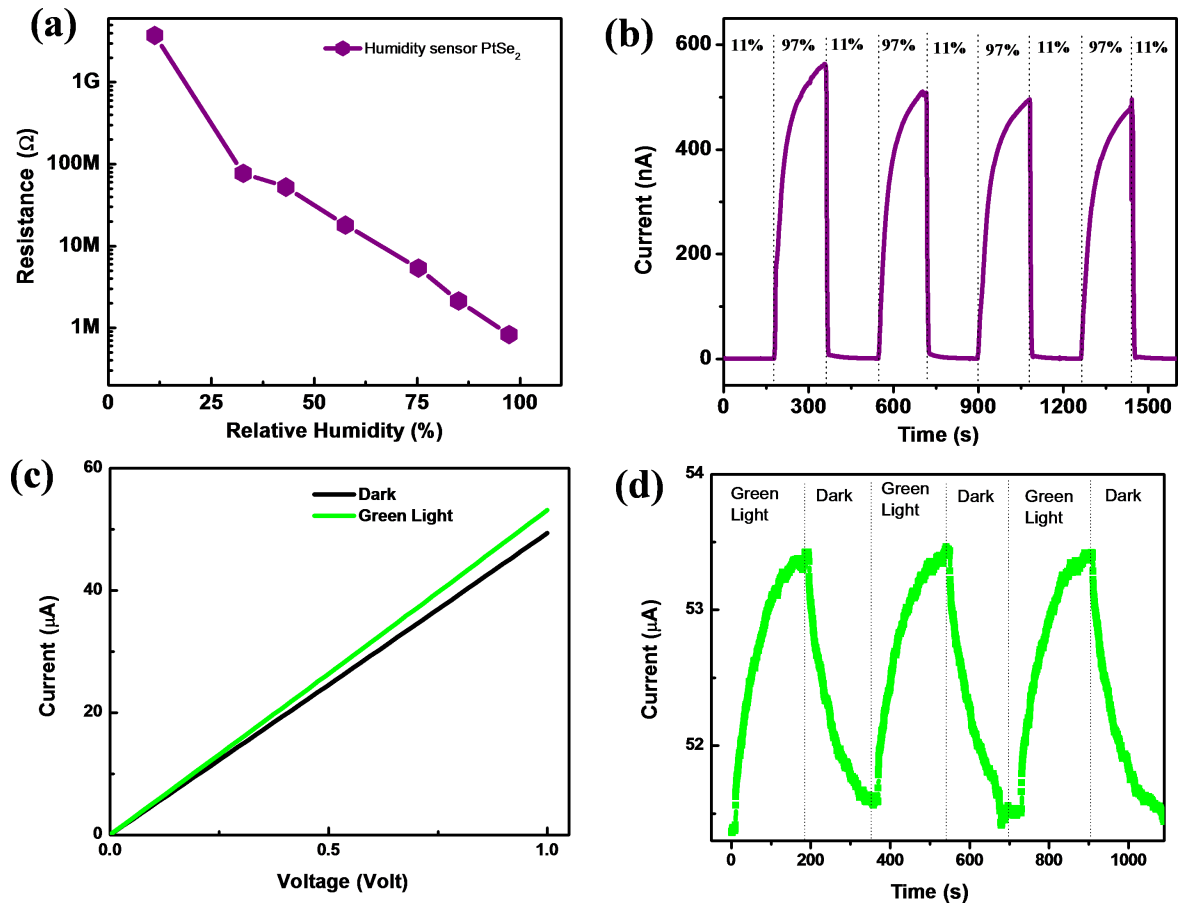

Figure 7: $PtSe_2$ nanosheet based humidity sensor: (a) Typical resistance versus relative humidity plot and (b) current–time (*I–t*) plot taken after switching 11% RH and 97% RH. The photodetector application of $PtSe_2$ nanosheets: (c) *I–V* in dark conditions and with green LED light and (d) typical *I–t* cycle when the LED is on and off, showing a favourable response.

mation of $PtSe_2$ nanosheets. Further, the XRD, Raman and SAED pattern results were used to analyze the crystal structure and to confirm the formation of the $PtSe_2$ phase. Temperature-dependent Raman spectroscopy investigations were carried out on $PtSe_2$ nanosheet films grown on Si substrates between 100–506 K. The temperature coefficient for the E_g and A_{1g} modes was found to be −0.014 and −0.008, respectively. A room temperature humidity sensor based on the $PtSe_2$ nanosheets demonstrated an excellent recovery time of ≈5 s, indicating the great potential of $PtSe_2$-based sensors for future nanoelectronics and sensor devices.

Supporting Information

Supporting Information File 1

Additional figures.
[https://www.beilstein-journals.org/bjnano/content/supplementary/2190-4286-10-46-S1.pdf]

Acknowledgements

This research work was supported by the SERB Government of India under the SERB Research Scientist scheme provided to Dr. D. J. Late.

ORCID® iDs

Mahendra S. Pawar - https://orcid.org/0000-0002-3642-3158
Dattatray J. Late - https://orcid.org/0000-0003-3007-7220

References

1. Geim, A. K.; Novoselov, K. S. *Nat. Mater.* **2007,** *6,* 183–191. doi:10.1038/nmat1849
2. Grigorenko, A. N.; Polini, M.; Novoselov, K. S. *Nat. Photonics* **2012,** *6,* 749–758. doi:10.1038/nphoton.2012.262
3. Stankovich, S.; Dikin, D. A.; Dommett, G. H. B.; Kohlhaas, K. M.; Zimney, E. J.; Stach, E. A.; Piner, R. D.; Nguyen, S. T.; Ruoff, R. S. *Nature* **2006,** *442,* 282–286. doi:10.1038/nature04969
4. Zhao, X.; Zhang, Q.; Chen, D.; Lu, P. *Macromolecules* **2010,** *43,* 2357–2363. doi:10.1021/ma902862u

5. Pawbake, A. S.; Mishra, K. K.; Machuno, L. G. B.; Gelamo, R. V.; Ravindran, T. R.; Rout, C. S.; Late, D. J. *Diamond Relat. Mater.* **2018,** *84,* 146–156. doi:10.1016/j.diamond.2018.03.021
6. Liu, W.; Luo, X.; Bao, Y.; Liu, Y. P.; Ning, G.-H.; Abdelwahab, I.; Li, L.; Nai, C. T.; Hu, Z. G.; Zhao, D.; Liu, B.; Quek, S. Y.; Loh, K. P. *Nat. Chem.* **2017,** *9,* 563–570. doi:10.1038/nchem.2696
7. Wang, Q. H.; Kalantar-Zadeh, K.; Kis, A.; Coleman, J. N.; Strano, M. S. *Nat. Nanotechnol.* **2012,** *7,* 699–712. doi:10.1038/nnano.2012.193
8. Peng, B.; Ang, P. K.; Loh, K. P. *Nano Today* **2015,** *10,* 128–137. doi:10.1016/j.nantod.2015.01.007
9. Li, H.; Shi, Y.; Chiu, M.-H.; Li, L.-J. *Nano Energy* **2015,** *18,* 293–305. doi:10.1016/j.nanoen.2015.10.023
10. Jariwala, D.; Sangwan, V. K.; Lauhon, L. J.; Marks, T. J.; Hersam, M. C. *ACS Nano* **2014,** *8,* 1102–1120. doi:10.1021/nn500064s
11. Shi, J.; Ma, D.; Han, G.-F.; Zhang, Y.; Ji, Q.; Gao, T.; Sun, J.; Song, X.; Li, C.; Zhang, Y.; Lang, X.-Y.; Zhang, Y.; Liu, Z. *ACS Nano* **2014,** *8,* 10196–10204. doi:10.1021/nn503211t
12. Voiry, D.; Salehi, M.; Silva, R.; Fujita, T.; Chen, M.; Asefa, T.; Shenoy, V. B.; Eda, G.; Chhowalla, M. *Nano Lett.* **2013,** *13,* 6222–6227. doi:10.1021/nl403661s
13. Splendiani, A.; Sun, L.; Zhang, Y.; Li, T.; Kim, J.; Chim, C.-Y.; Galli, G.; Wang, F. *Nano Lett.* **2010,** *10,* 1271–1275. doi:10.1021/nl903868w
14. Tongay, S.; Zhou, J.; Ataca, C.; Lo, K.; Matthews, T. S.; Li, J.; Grossman, J. C.; Wu, J. *Nano Lett.* **2012,** *12,* 5576–5580. doi:10.1021/nl302584w
15. Zhang, Y.; Chang, T.-R.; Zhou, B.; Cui, Y.-T.; Yan, H.; Liu, Z.; Schmitt, F.; Lee, J.; Moore, R.; Chen, Y.; Lin, H.; Jeng, H.-T.; Mo, S.-K.; Hussain, Z.; Bansil, A.; Shen, Z.-X. *Nat. Nanotechnol.* **2014,** *9,* 111–115. doi:10.1038/nnano.2013.277
16. Mak, K. F.; Lee, C.; Hone, J.; Shan, J.; Heinz, T. F. *Phys. Rev. Lett.* **2010,** *105,* 136805–136808. doi:10.1103/physrevlett.105.136805
17. Sundaram, R. S.; Engel, M.; Lombardo, A.; Krupke, R.; Ferrari, A. C.; Avouris, P.; Steiner, M. *Nano Lett.* **2013,** *13,* 1416–1421. doi:10.1021/nl400516a
18. Guo, G. Y.; Liang, W. Y. *J. Phys. C: Solid State Phys.* **1986,** *19,* 995–1008. doi:10.1088/0022-3719/19/7/011
19. Wang, Y.; Li, L.; Yao, W.; Song, S.; Sun, J. T.; Pan, J.; Ren, X.; Li, C.; Okunishi, E.; Wang, Y.-Q.; Wang, E.; Shao, Y.; Zhang, Y. Y.; Yang, H.-t.; Schwier, E. F.; Iwasawa, H.; Shimada, K.; Taniguchi, M.; Cheng, Z.; Zhou, S.; Du, S.; Pennycook, S. J.; Pantelides, S. T.; Gao, H.-J. *Nano Lett.* **2015,** *15,* 4013–4018. doi:10.1021/acs.nanolett.5b00964
20. Zhao, Y.; Qiao, J.; Yu, Z.; Yu, P.; Xu, K.; Lau, S. P.; Zhou, W.; Liu, Z.; Wang, X.; Ji, W.; Chai, Y. *Adv. Mater. (Weinheim, Ger.)* **2017,** *29,* 1604230. doi:10.1002/adma.201604230
21. Sattar, S.; Schwingenschlögl, U. *ACS Appl. Mater. Interfaces* **2017,** *9,* 15809–15813. doi:10.1021/acsami.7b00012
22. O'Brien, M.; McEvoy, N.; Motta, C.; Zheng, J.-Y.; Berner, N. C.; Kotakoski, J.; Elibol, K.; Pennycook, T. J.; Meyer, J. C.; Yim, C.; Abid, M.; Hallam, T.; Donegan, J. F.; Sanvito, S.; Duesberg, G. S. *2D Mater.* **2016,** *3,* 021004. doi:10.1088/2053-1583/3/2/021004
23. Grønvold, F.; Haraldsen, H.; Kjekshus, A.; Söderquist, R. *Acta Chem. Scand.* **1960,** *14,* 1879–1893. doi:10.3891/acta.chem.scand.14-1879
24. Yim, C.; Lee, K.; McEvoy, N.; O'Brien, M.; Riazimehr, S.; Berner, N. C.; Cullen, C. P.; Kotakoski, J.; Meyer, J. C.; Lemme, M. C.; Duesberg, G. S. *ACS Nano* **2016,** *10,* 9550–9558. doi:10.1021/acsnano.6b04898
25. Ali Umar, A.; Md Saad, S. K.; Mat Salleh, M. *ACS Omega* **2017,** *2,* 3325–3332. doi:10.1021/acsomega.7b00580
26. Erande, M. B.; Pawar, M. S.; Late, D. J. *ACS Appl. Mater. Interfaces* **2016,** *8,* 11548–11556. doi:10.1021/acsami.5b10247
27. Yu, X.; Yu, P.; Wu, D.; Singh, B.; Zeng, Q.; Lin, H.; Zhou, W.; Lin, J.; Suenaga, K.; Liu, Z.; Wang, Q. J. *Nat. Commun.* **2018,** *9,* 1545. doi:10.1038/s41467-018-03935-0
28. Zhang, K.; Yan, M.; Zhang, H.; Huang, H.; Arita, M.; Sun, Z.; Duan, W.; Wu, Y.; Zhou, S. *Phys. Rev. B* **2017,** *96,* 125102. doi:10.1103/physrevb.96.125102
29. Pawbake, A. S.; Pawar, M. S.; Jadkar, S. R.; Late, D. J. *Nanoscale* **2016,** *8,* 3008–3018. doi:10.1039/c5nr07401k
30. Late, D. J.; Maitra, U.; Panchakarla, L. S.; Waghmare, U. V.; Rao, C. N. R. *J. Phys.: Condens. Matter* **2011,** *23,* 055303. doi:10.1088/0953-8984/23/5/055303
31. Late, D. J. *ACS Appl. Mater. Interfaces* **2015,** *7,* 5857–5862. doi:10.1021/am509056b
32. Pawbake, A. S.; Island, J. O.; Flores, E.; Ares, J. R.; Sanchez, C.; Ferrer, I. J.; Jadkar, S. R.; van der Zant, H. S. J.; Castellanos-Gomez, A.; Late, D. J. *ACS Appl. Mater. Interfaces* **2015,** *7,* 24185–24190. doi:10.1021/acsami.5b07492
33. Calizo, I.; Balandin, A. A.; Bao, W.; Miao, F.; Lau, C. N. *Nano Lett.* **2007,** *7,* 2645–2649. doi:10.1021/nl071033g
34. Late, D. J. *Appl. Mater. Today* **2016,** *5,* 98–102. doi:10.1016/j.apmt.2016.09.013
35. Pawar, M.; Kadam, S.; Late, D. J. *ChemistrySelect* **2017,** *2,* 4068–4075. doi:10.1002/slct.201700261
36. Late, D. J.; Huang, Y.-K.; Liu, B.; Acharya, J.; Shirodkar, S. N.; Luo, J.; Yan, A.; Charles, D.; Waghmare, U. V.; Dravid, V. P.; Rao, C. N. R. *ACS Nano* **2013,** *7,* 4879–4891. doi:10.1021/nn400026u
37. Late, D. J.; Doneux, T.; Bougouma, M. *Appl. Phys. Lett.* **2014,** *105,* 233103. doi:10.1063/1.4903358

License and Terms